



Incorporation of anthocyanin into zein nanofibrous films by electrospinning: Structural characterization, functional properties, and ammonia color-responsiveness

Jun Wang^{a,b,1}, Wenpeng Zhao^{b,c,1}, Dongli Qin^b, Hongyan Shan^b, Xiaoman Zhu^a, Lilan Chen^c, Ying Liu^{a,*}, Songnan Li^{d,*}

^a State Key Laboratory of Food Nutrition and Safety, College of Biotechnology, Tianjin University of Science and Technology, Tianjin 300457, China

^b School of Tourism and Cuisine, Yangzhou University, Yangzhou 225127, China

^c Institutes of Sichuan Cuisine Development and Dietary Culture, Sichuan Tourism University, Chengdu 610100, China

^d Joint International Research Laboratory of Agriculture and Agri-Product Safety of the Ministry of Education of China, Institutes of Agricultural Science and Technology Development, Yangzhou University, Yangzhou 225009, China

ARTICLE INFO

Keywords:

Freshness-indicating label
Green electrospinning
Fibrous film
Color-responsiveness
Intelligent food packaging

ABSTRACT

Green electrospinning for the production of freshness-indicating labels, employing entirely natural biopolymers and pigments, holds significance in the development of intelligent food packaging. This study aimed to prepare zein (Z) fibrous film (FF) incorporated with varying concentrations of anthocyanin (A; 0–0.5 %) through green electrospinning. Furthermore, we evaluated their structural characteristics, functional properties, and color responsiveness to ammonia. With an increase in A concentration from 0 % to 0.5 %, the average thickness and fiber diameter of the electrospun Z-FF increased from 68.6 μm to 102.0 μm and from 582.1 nm to 690.7 nm, respectively. At A concentration of 0.2 %, the A content and loading efficiency of electrospun ZA-FF exhibited the most optimal values (6.8 mg/g and 39.4 %). Surface hydrophobicity, thermodynamic properties, and mechanical characteristics of ZA-FF were significantly improved, attributable to changes in their secondary and crystal structures from the interaction of Z and A. In the ammonia color-responsiveness test, an obvious color change with ΔE values of 13.1 and 20.0 was observed for Z-FF incorporated with A at concentrations of 0.2 % and 0.5 %, respectively. This study provides novel insights into the development of Z-based freshness-indicating labels via green electrospinning for intelligent food packaging, especially in livestock and marine products.

1. Introduction

Seafood and meat represent crucial sources of most nutrients, such as proteins, fatty acids, vitamins, and minerals, which confer benefits to human health. However, these food items are highly perishable, with microbial spoilage, particularly by pathogenic microorganisms, and the resultant harmful substances, potentially leading to foodborne illnesses (Lee & Yoon, 2021). Therefore, the implementation of indicating labels capable of monitoring the freshness of foods throughout their manufacturing, storage, and consumption stages is of considerable importance. Concerning protein-rich foods, the activity of microorganisms induces the production of volatile amines and pH alterations, which provide valuable insights into their freshness, quality, and safety

(Panjagari, Raman, Uma, Suwalka, & Thomas, 2021). Consequently, intelligent indicating labels incorporating pH-sensitive dyes have been devised to detect total volatile basic nitrogen (TVB-N), facilitating real-time and visual monitoring of freshness by eliciting a color change upon pH increase (Erna, Rovina, & Mantihal, 2021). Previous studies have demonstrated that various pH-sensitive freshness-indicating labels can be prepared by mixing anthocyanins (A) with film-forming polymer solutions through solvent casting (Chen, Zhang, Bhandari, & Yang, 2020; Shen, Zhang, Mujumdar, & Ma, 2023). However, this current technological approach is not suitable for large-scale production owing to its low efficiency, low indication sensitivity, and potential environmental pollution.

Electrospinning is a fiber production technology wherein polymer

* Corresponding authors.

E-mail addresses: yingliu@mail.tust.edu.cn (Y. Liu), lsnyz2020@yzu.edu.cn (S. Li).

¹ These authors contributed equally to this work.

solutions or melts are evaporated, stretched, and solidified into micro-and/or nanofibers under high-voltage electrostatic forces (Li et al., 2021). Compared with traditional food packaging materials, electrospun nanofibers exhibit high porosity and specific surface area, rendering them suitable for the development of intelligent indicating labels (Guo et al., 2022). Han et al. (2023) prepared an intelligent indicating label using polyvinyl alcohol/silver/grape seed A through electrospinning, demonstrating visible color changes from red to yellow when employed to monitor the freshness of pork. Lv et al. (2024) electrospun a freshness-indicating label using octenyl succinic anhydride starch/polyvinyl alcohol/roselle A for visual monitoring of shrimp, exhibiting visible color changes from red, purple, to dark green in response to freshness variations from fresh, sub-fresh, and spoilage, respectively. He et al. (2023) fabricated a novel A electrospun fibrous film (FF) through caffeic acid co-pigmentation with polyacrylonitrile, displaying discernible visual color changes from pink to light purple during fish storage at 4 °C.

Although electrospinning for the preparation of freshness-indicating labels has been extensively studied, its application has been limited by environmental concerns and food safety issues arising from the utilization of chemical synthetic polymers and/or pH-sensitive dyes. Hence, green electrospinning holds significant promise for a wide range of applications in the field of food packaging for freshness-indicating labels. Among various bio-based polymers, zein (Z), the major storage protein of corn and an important industrial byproduct of ethanol production, exhibits favorable film-forming properties, excellent hydrophobicity, and is both biodegradable and biocompatible, making it suitable for use in food packaging (Garavand et al., 2024). As water-soluble edible natural pigments widely found in fruits, vegetables, and flowers, anthocyanins (A) can serve as ideal pH colorimetric indicators for freshness-indicating labels owing to their abundance, favorable food safety, and high pH sensitivity (Lova, 2021). Therefore, this study aimed to prepare Z nano-FFs incorporated with varying concentrations of A (0–0.5 %) through green electrospinning as a novel approach for freshness-indicating labels. A digital camera, thickness instrument, scanning electron microscopy (SEM) in conjunction with Image J software, Fourier transform infrared (FT-IR) spectroscopy, and X-ray diffraction (XRD) were employed to assess their structural characteristics. Furthermore, we evaluated their functional properties using a spectrophotometer, a contact angle instrument, a thermogravimetric analyzer (TGA), and a dynamic mechanical analyzer (DMA). Additionally, we further explored their antioxidant properties, storage stability, and color-responsiveness to ammonia for their potential utilization in indicating food freshness.

2. Materials and methods

2.1. Materials

Z (92 % purity) was procured from Shanghai Yuanye Biotechnology Technology Co., Ltd. (Shanghai, China). A (36 % purity) from blueberry extract was obtained from Shandong Shengjiade Biotechnology Co., Ltd. (Jining, China). Anhydrous ethanol and ammonia solutions were purchased from Sinopharm Chemical Reagent Co., Ltd. (Shanghai, China). All other chemicals utilized in this study were of analytical grade.

2.2. Dope preparation

The preparation of Z-based dope followed a previously established method (Khalafi, Gharachorloo, Ganjloo, & Yousefi, 2023) with minor modifications. Following our preliminary experiment for the optimization solubility, a series of A solutions was prepared by dissolving varying concentrations of A (5, 10, 20, and 50 mg) into 10 mL of an ethanol aqueous solution (80 %, v/v). Subsequently, 2.5 g of Z was introduced with magnetic stirring to yield Z-based dope, designated as ZA0.05, ZA0.1, ZA0.2, and ZA0.5, respectively.

2.3. Electrospinning

The aforementioned dope was loaded into a 10 mL syringe and subsequently affixed within an electrospinning instrument (JDF05, Nano Apparatus Technology Co., Ltd., Changsha, China). Based on a previous study (Huang et al., 2024), the electrospinning parameters employed were as follows: a voltage of 17 kV, a feed speed of 0.3 mL/h, a collecting distance of 12 cm, blunt needles with a gauge of 23G, a collecting drum rotating at 5 rpm, and an environmental temperature and humidity range of 25–30 °C and 45–55 %, respectively. After electrospinning for 10 h, FF was obtained and subsequently stored in a dryer at 25 °C until further analysis.

2.4. Structural characterization of FF

2.4.1. Macroscopic examination and thickness distribution

The aforementioned FF was photographed for macroscopic examination using a digital camera (Z30, Nikon, Tokyo, Japan), while changes in its color were recorded using a colorimeter (Caipu Technology Co., Ltd., Hangzhou, China). Subsequently, 25 points were uniformly marked across the surface of FF and subsequently assessed for thickness utilizing a thickness measurement instrument (Shengtaixin Electronic Technology Co., Ltd., Huzhou, China).

2.4.2. Microscopic examination and fiber diameter distribution

A sample (0.5 cm in length × 0.5 cm in width) was subjected to gold-spraying to facilitate SEM analysis, with the instrument (S-4800, Hitachi, Tokyo, Japan) operating at an accelerating voltage of 10 kV (Li et al., 2022). Magnifications of 5,000 and 20,000 were employed for the examination of the overall microstructure and the analysis of fiber diameter distribution in FF using Image J software (National Institutes of Health, Bethesda, MD, USA), respectively.

2.4.3. FT-IR analysis

Samples were analyzed using a FT-IR spectrometer (Nicolet IS50, Thermo Fisher, Waltham, MA, USA), scanning within the range of 400–4000 cm⁻¹, employing 32 scans (Li et al., 2021).

2.4.4. XRD analysis

Samples were analyzed over a 2θ range of 4–40 ° at a scanning rate of 0.5 °/min, utilizing Cu-Kα radiation using an XRD instrument (D8 Advance, Bruker, Berlin, Germany) (Li et al., 2018).

2.5. Functional properties of FF

2.5.1. Evaluation of anthocyanin incorporation

The evaluation of anthocyanin (A) incorporation was conducted following established methods (Li et al., 2018; Li, Huang, et al., 2021) with minor modifications. A sample (50 mg, dry weight) was dissolved in 10 mL of an 80 % ethanol aqueous solution, thoroughly vortexed for 5 min, then centrifuged at 6000 g for 5 min, after which the supernatant was collected. The concentration of A was determined from the absorbance-concentration curve by measuring at a wavelength of 540 nm (the maximum absorption wavelength of A as determined by full-band scanning) using an ultraviolet-visible spectrophotometer (Persee, Beijing, China). The content (X, mg/g) and loading efficiency (Y, %) of A were calculated using Eqs. (1) and (2).

$$X = \frac{C \times V \times M_1 \times 1000}{50} \quad (1)$$

$$Y = \frac{X}{M_2} \times 100 \quad (2)$$

where C (mg/g) represents the concentration of A, V (mL) denotes the volume of the sample solution, M₁ (g) signifies the total mass of the as-spun sample, and M₂ (g) denotes the total mass of A added before

electrospinning.

2.5.2. Contact angle measurement

The water contact angle (WCA) of a sample was determined via the pendent drop method utilizing a contact angle instrument (JY-82C, Dingsheng Testing Machine Co., Ltd., Chengde, China) (Li, Zhu, et al., 2021).

2.5.3. TGA measurement

The thermal properties of a sample were analyzed using a TGA (Pyris 1, PerkinElmer Inc., Shelton, CT, USA) within the temperature range of 30–800 °C at a rate of 20 °C/min (Narayanan, Mani, & Thambusamy, 2020).

2.5.4. DMA measurement

The mechanical performance of a sample (3 cm in length \times 0.4 cm in width) was evaluated using a DMA (DMA Q800, TA Instruments, New Castle, Delaware, USA) (Ciarfaglia et al., 2021).

2.6. Color-responsiveness to ammonia

The color responsiveness of a sample to ammonia was evaluated using a previously reported method (Wu, Liu, Zhou, & Shao, 2024a). A sample (1 cm in length \times 1 cm in width) was placed 3 cm above the top of a bottle containing 25 % (v/v) ammonia for 20 min. Subsequently, the color change of the sample was examined as described in Section 2.4.1. The total color difference (ΔE) of a sample was calculated using Eq. (3).

$$\Delta E = \sqrt{(L^* - L_0^*)^2 + (a^* - a_0^*)^2 + (b^* - b_0^*)^2} \quad (3)$$

where L^* , a^* , and b^* represent the color parameters of the sample following the aforementioned ammonia treatment, and L_0^* , a_0^* , and b_0^* denote the original color parameters of the sample.

2.7. Statistical analysis

All measurements were independently repeated three times in the experiments, and the results are presented as the mean value and the standard deviation. Analysis of variance was conducted utilizing Duncan's multiple-range test ($p < 0.05$) using statistical software (SPSS Inc., Chicago, IL, USA).

3. Results and discussion

3.1. Structural characteristics of FF

3.1.1. Macrostructures

Fig. 1A illustrates the appearance of Z-FFs as a function of A concentration (0–0.5 %). All electrospun Z-FF incorporated with A at a concentration of 0–0.5 % exhibited a smooth surface without obvious transparent “droplet”, indicative of the novel electrospinning formulation (25 % [w/v] Z dissolved in an 80 % [w/v] ethanol aqueous solution) and process parameters utilized in this study. As the concentration of A increased from 0 % to 0.5 %, the color of the Z-FF transitioned from white to pink, accompanied by a notable rise in the a^* value from -0.3 to 7.2 . This phenomenon aligns with the findings of a previous study that involved electrospinning Z with an anthocyanic extract of jambolan (Dos Santos et al., 2023).

As shown in Fig. 1B, as the concentration of A increased from 0 % to 0.5 %, the thickness distribution color of the electrospun Z-FF changed from light blue to dark blue, with the average thickness expanding from $68.6 \mu\text{m}$ to $102.0 \mu\text{m}$, implying their favorable electrospinning efficiency. During the electrospinning, solidified nanofibers after solvent evaporated could deposit on the collector layer by layer to form a fibrous film, where electrospinning efficiency could be evaluated from its average thickness (Li, Zhu, et al., 2021).

3.1.2. Microstructures

Fig. 1C presents SEM images of fiber diameters for Z-FFs as a function of A concentration (0–0.5 %). All electrospun Z-FF with A at a

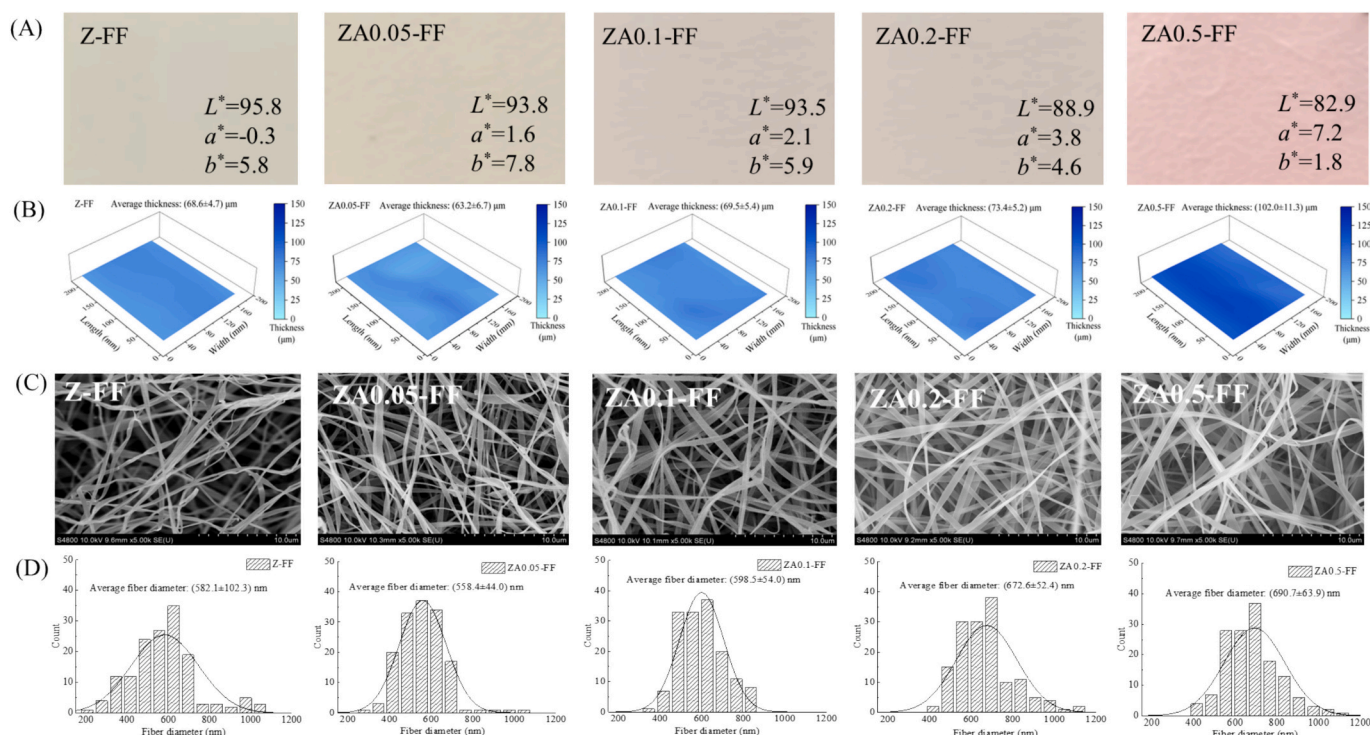


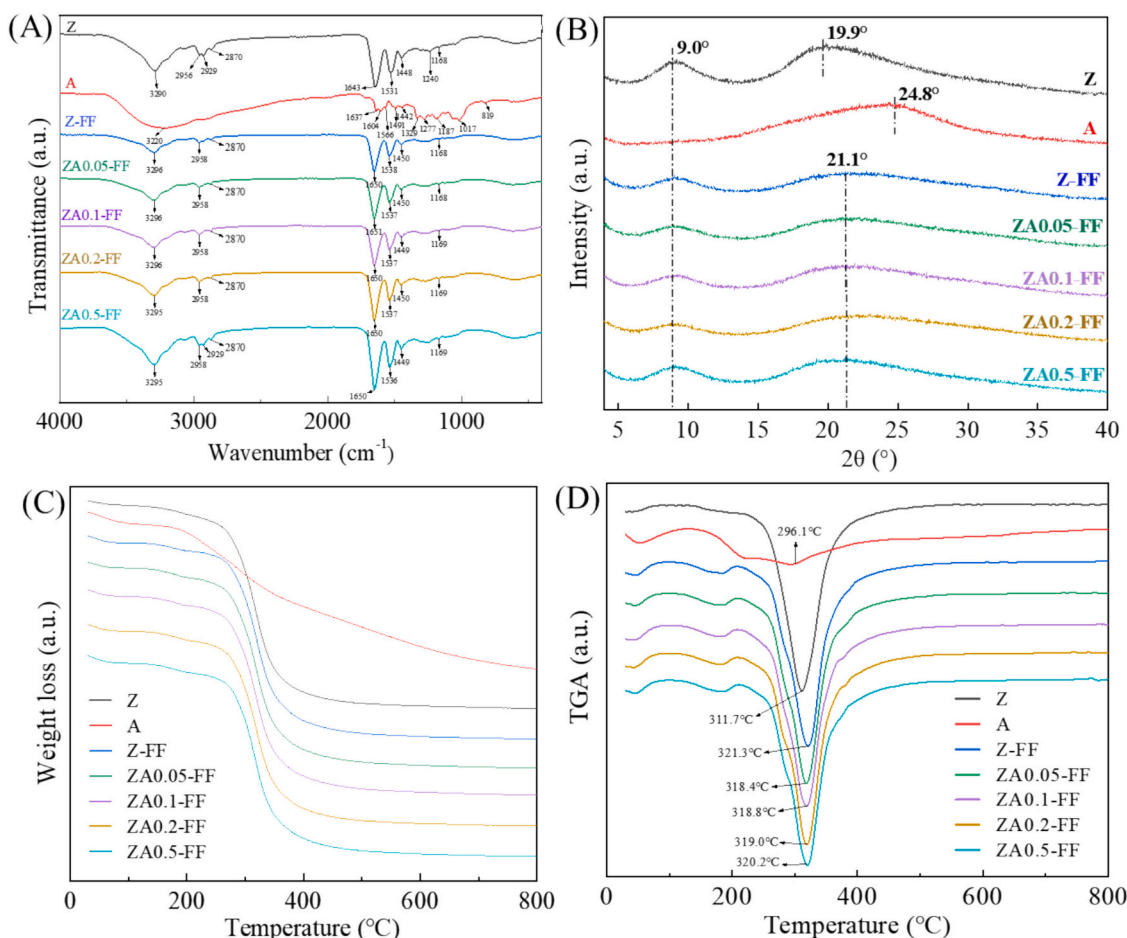
Fig. 1. Appearances (A), thickness distributions (B), SEM images (C) and fiber diameter distributions (D) of Z-FFs as a function of A addition (0–0.5 %).

concentration of 0–0.5 % presented a smooth, flat, bead-free, and ribbon-like morphology, reminiscent of the characteristics observed in electrospun Z/propolis nanofibers derived from 70 % ethanolic solutions (Moradkhannejhad, Abdouss, Nikfarjam, Mazinani, & Heydari, 2018). And their more nano-size morphologies could be further exhibited in Fig. S4 with higher magnification (10,000 \times and 20,000 \times). As shown in Fig. 1D, analysis of fiber diameter distribution demonstrated that the average fiber diameter of electrospun Z-FF increased from 582.1 nm to 690.7 nm with increasing concentrations of A from 0 % to 0.5 %, implying a nanoscale dimension. A similar result was also found in the electrospun Z/tannic acid composite FF with average fiber diameters ranging from 684 to 1060 nm using a 70 % ethanolic solution when tannic acid concentration increased from 0.5 % to 1 % (Luduvico et al., 2024). Concerning the consistent electrospinning parameters (voltage, feed speed, and collecting distance) and environmental conditions (temperature and humidity), the aforementioned results could be influenced by their electrospinning solution properties (mainly viscosity and conductivity), which was closely linked to the formation of the Taylor cone (Kailasa et al., 2021). Appropriate viscosity and conductivity could enhance electrospinning process by promoting polymer stretching, resulting in the increased fiber diameter (Angel, Li, Yan, & Kong, 2022). Additionally, viscosity and conductivity of the electrospinning solution from Z-FF as a function of A concentration (0–0.5 %) are shown in Table S1. There is an increasing trend in viscosity from 340.50 mPa·s to 355.67 mPa·s with the increasing A concentration from 0 % to 0.2 %, implying the enhanced molecular entanglement between Z and increased A. Further increasing A concentration to 0.5 %, it exhibited a decreased value (348.36 mPa·s), resulting from the excess A prohibited the comparable molecular interaction of polymer chains

(Rostamabadi, Assadpour, Tabarestani, Falsafi, & Jafari, 2020). Moreover, conductivity of Z-FF electrospinning solution increased from 88.17 $\mu\text{m/s}$ to 99.53 $\mu\text{m/s}$ with the increased A concentration from 0 % to 0.2 %, which should be associated with the presence of numerous phenols in its structure (Khoshnoudi-Nia, Sharif, & Jafari, 2020). However, no significant increase was observed for conductivity when A concentration further increased to 0.5 %, which was likely due to zein saturation, similar to that of tannic acid-loaded Z-FF (Luduvico et al., 2024). The above characteristic changes were a critical factor in the sufficient molecular entanglement and stable jet eruption, which should be responsible for the following structural characterization and functional properties (Angel et al., 2022).

3.1.3. Secondary structures

Fig. 2A illustrates the FT-IR analysis of Z-FFs as a function of A concentration (0–0.5 %) in conjunction with Z and A. The broad peak observed in Z, ranging from 3290 cm^{-1} to 3295 cm^{-1} , signifies the stretching vibration of the N–H bond, characteristic of proteins. Additionally, the stretching vibrations of the N–H, C=O, and C–N bonds, along with the bending vibration of the N–H bond in Z, were observed at 3290 cm^{-1} , 1643 cm^{-1} , 1531 cm^{-1} , and 1168 cm^{-1} , respectively, consistent with prior research conducted by Krumreich et al. (2019). The absorption peak of A at 3220 cm^{-1} corresponds to the absorption of unsaturated C–H stretching vibrations, similar to those observed in purple cabbage A, as noted by Pakolpakçil et al. (2021). After electrospinning, the spectrum of Z-FF exhibited a C=O stretching vibration at 1643–1651 cm^{-1} (amide I band), an in-plane bending vibration of the N–H bond at 1531–1538 cm^{-1} (amide II band), and a bending vibration of the C–N bond at 1168–1169 cm^{-1} (amide III band). At varying



concentrations of A (0.05–0.5 %), the stretching vibrations of the N—H, C=O, and C—N bonds and the bending vibration of the N—H bond in ZA-FF, exhibited slight shifts towards higher wavenumbers, approximately at 3296 cm⁻¹, 1650 cm⁻¹, 1537 cm⁻¹, and 1169 cm⁻¹, respectively. These shifts indicated the formation of hydrogen bonds between Z and A. No apparent differences in wavenumber characteristics were observed between Z-FF and ZA-FF, which could be attributed to the masking effect of Z resulting from the low concentrations of A (≤ 0.5 %). Similar findings have been reported in the electrospinning of ZA-FF with gelatin and Fe²⁺ (Gao et al., 2022).

FT-IR analysis of Z-FFs as a function of A concentration (0–0.5 %) and Z elucidated their secondary structure, as summarized in Table 1. The proportions of α -helix, β -fold, and β -turn in Z were 27.2 %, 46.2 %, and 26.6 %, respectively, with no random coil structure detected, consistent with the findings reported by Seong et al. (2016). Compared to Z, electrospun Z-FF exhibited a significant increase in the proportion of α -helix (28.2 %) and β -turn (28.1 %), with a significantly decreased proportion of β -fold (43.7 %). A similar trend was observed in Z electrospinning with varying concentrations of A (0.05–0.5 %), indicating a transition from an ordered structure (α -helix + β -turn) to a more disordered structure (β -fold + random coil). Among ZA-FF, ZA0.5-FF displayed the lowest proportion of α -helix (15.7 %) and the highest proportion of β -turn (31.1 %), suggesting that higher A concentrations favored the formation of a more ordered structure.

3.1.4. Crystal structures

Fig. 2B illustrates the XRD spectrum of Z-FFs in relation to varying concentrations of A (0–0.5 %) in conjunction with Z and A. Two broad diffraction peaks at 9.0° and 19.9° were observed for Z, consistent with the findings of previous studies (Gholizadeh et al., 2024; Li, Huang, et al., 2021). Conversely, the diffraction pattern of A exhibited a flattened peak at 24.8°, indicative of its amorphous structure. Compared to Z, Z-FF exhibited a shifted broad peak from 19.9° to 21.1°, indicating changes in crystal structures subsequent to electrospinning. This phenomenon has also been observed in electrospinning experiments employing a Z 35 % concentration and an 80 % ethanolic solution (Aytac, Ipek, Durgun, & Uyar, 2018). No apparent differences in XRD characteristic peaks were observed among ZA-FF with varying A concentrations (0.05–0.5 %), consistent with corresponding FT-IR data. Both sets of data indicated a greater prevalence of amorphous structures following Z electrospinning with A. Similar outcomes have been reported by studies investigating the electrospinning of Z with varying A concentrations (2.5–4.5 %) (Khalafi et al., 2023).

Table 1
Secondary structures of Z-FFs as a function of A addition (0–0.5 %) and Z.

Samples	α -helix (%)	β -fold (%)	Random coil (%)	β -turn (%)	Ordered structure (α -helix + β -turn) (%)
Z	27.2 ± 0.3 ^b	46.2 ± 1.8 ^a	n.d.	26.6 ± 1.5 ^c	53.8
Z-FF	28.2 ± 4.0 ^a	43.7 ± 6.5 ^b	n.d.	28.1 ± 2.5 ^b	56.3
ZA0.05-FF	21.9 ± 2.4 ^c	34.7 ± 3.6 ^d	27.3 ± 1.1 ^a	16.0 ± 2.4 ^d	37.9
ZA0.1-FF	27.5 ± 5.5 ^b	22.1 ± 1.4 ^e	24.8 ± 2.4 ^b	25.5 ± 1.1 ^c	53.0
ZA0.2-FF	27.0 ± 4.7 ^b	36.0 ± 5.4 ^d	13.2 ± 1.8 ^c	23.8 ± 8.6 ^{bc}	50.8
ZA0.5-FF	15.7 ± 2.2 ^d	38.8 ± 5.0 ^c	14.3 ± 2.0 ^c	31.1 ± 3.1 ^a	46.8

n.d.: not detected.

3.2. Functional properties of FF

3.2.1. A content and loading efficiency

The A content and loading efficiency in Z-FFs in relation to the concentration of A (0–0.5 %) is shown in Table 2. As the A concentration increased from 0.05 % to 0.5 %, the A content in the ZA-FF significantly increased from 3.4 to 14.7 mg/g, with a significant decrease in loading efficiency from 76.8 % to 37.6 %. This decrease can be attributed to an insufficient amount of Z (2.5 g) when the A concentration exceeded 0.2 %. At a 0.2 % concentration of A, the A content and loading efficiency reached their optimum values (6.8 mg/g and 39.4 %). Similar results have been reported by Dos Santos et al. (2023) who loaded 20–40 % of anthocyanic extract of jambolana into electrospun Z-FF, as well as by Li, Zhu, et al. (2021), who fabricated starch/Z nanocomposites via starch nanoprecipitation.






3.2.2. Surface hydrophobicity

The WCA of Z-FFs as a function of A concentration (0–0.5 %) is shown in Table 2. The WCA of Z-FF measured 134.5°, exceeding 90°, indicative of its robust hydrophobicity, likely attributable to its inherent abundance of hydrophobic amino acids (Plath et al., 2021). This result is similar to that (135.7°) obtained by He, Jiang, Wang, Xie, and Zhao (2017) in their study on electrospun Z-FF derived from an 80 % ethanolic solution. Compared with that of Z-FF, the WCA of ZA0.05-FF significantly decreased to 118.4°, due to the hydrophilicity of A molecules increasing the interaction of the nanofibers with water drop (Dos Santos et al., 2023). Generally, higher A concentration could lead to greater wettability of FF with lower WCA values, evidenced from that of Z-FF loaded with red onion bulb extract (Cruz et al., 2024). Although theoretically, ZA-FF exhibited a gradual increase as the concentration of A rose from 0.05 % to 0.5 %. This was likely due to zein saturation above 0.25 % concentration, resulting in the variation in the proportion of secondary structures affecting their hydrophilicity by capillary effect (Merz et al., 2020). A similar result was reported from that of Z-FF rising from 59.6° to 116.9°, closely associated with the increasing transition from β -sheet to α -helix structures as the Z concentration increased from 15 % to 25 % (Luo, Saadi, Fu, Taxipalati, & Deng, 2021). In addition, their surface roughness, morphology, diameter and porosity should also be considered along with surface tension in future studies to gain a better understanding of the underlying mechanisms.

3.2.3. Thermodynamic properties

Fig. 2C and 2D illustrate TGA (C) and derivative thermogravimetry (DTG; D) curves depicting the impact of A concentration (0–0.5 %) on Z, A, and Z-FFs. The TGA curve of A primarily exhibited two distinct stages: 1) 30–180 °C, with a weight loss rate of 6.8 %, attributed to residual water and/or solvent evaporation; and 2) 180–800 °C, with a weight loss rate of 60.7 %, attributed to the thermal degradation of A. In contrast,

Table 2
A content, loading efficiency, water contact angle of Z-FFs as a function of A addition (0–0.5 %).

Samples	A content	Loading efficiency	Water drop image	Contact angle (°)
Z-FF	n.d.	n.d.		134.5 ± 1.5 ^a
ZA0.05-FF	3.4 ± 0.1 ^d	76.8 ± 1.1 ^a		118.4 ± 1.8 ^b
ZA0.1-FF	4.4 ± 0.2 ^c	43.0 ± 1.7 ^b		120.8 ± 5.1 ^b
ZA0.2-FF	6.8 ± 0.5 ^b	39.4 ± 2.7 ^c		121.0 ± 0.6 ^b
ZA0.5-FF	14.7 ± 0.2 ^a	37.6 ± 0.6 ^c		125.7 ± 7.3 ^{ab}

n.d.: not detected.

thermal degradation of Z, Z-FF, and ZA-FF occurred at 30–80 °C and 260–370 °C, with varying degrees of residual content. As the temperature increased from 370 °C to 800 °C, the residual amount of Z-FF was 12.3 %, higher than that of Z (10.7 %), indicating enhanced interaction of Z molecules and improved thermal stability (Wan, Wang, Yang, Guo, & Yin, 2016). Compared with Z-FF, upon increasing A concentration from 0.05 % to 0.5 %, the residual amount of ZA-FF initially decreased and then increased (11.4 %, 11.5 %, 13.1 %, and 13.5 %). As shown in Fig. 2D, corresponding changes in thermal degradation were evident from their maximum weight loss rate temperature (MWLRT) in the DTG curve. MWLRT for Z-FF was 321.3 °C, higher than that of Z (311.7 °C) but lower than that of ZA-FF (318.4–320.2 °C) with A at concentrations of 0.05–0.5 %. These results may be attributed to the degree of intermolecular interaction (such as hydrogen bonds and van der Waals forces) between Z and A (Prietto et al., 2017), as supported by their FT-IR data.

3.2.4. Mechanical properties

Fig. 3 presents the mechanical properties (A: stress-strain curves; B: tensile strength; C: elongation; D: Young's modulus) of Z-FFs as a function of A concentration (0–0.5 %). With escalating strain, the stress in Z-FF and ZA-FF increased gradually, as shown in Fig. 3A. Further analysis of the stress-strain curves facilitated the derivation of three important mechanical parameters—tensile strength, elongation at break, and Young's modulus—essential for evaluating the tensile and ductility of food packaging materials (Wang et al., 2016). As the A concentration increased from 0 % to 0.2 %, the tensile strength of Z-FF increased significantly from 0.46 MPa to 0.87 MPa, subsequently declining to 0.65 MPa upon increasing the A concentration to 0.5 % (Fig. 3B). This phenomenon may be associated with the concentration of A within Z-FF, whereby a lower A concentration promoted intermolecular interactions between Z and A, whereas higher concentrations of A

increased the likelihood of agglomeration of A molecules (Julien et al., 2019). Elongation at break denotes the elongation length ratio of a fiber post-stretching to the initial length when subjected to external force, expressed as the strain corresponding to fracture. Regarding elongation at break of Z-FF and ZA-FF (Fig. 3C), ZA0.2-FF exhibited the lowest value (2.21 %), potentially linked to limited interaction forces between A and Z owing to relatively high A content. Young's modulus is the ratio of fiber stress to strain, which is typically used to represent the ability of solid materials to resist deformation. Regarding Young's modulus for Z-FF and ZA-FF (Fig. 3D), a trend emerged, characterized by an initial increase (11.27 to 29.10 MPa across an A concentration of 0–0.2 %) followed by a decrease (22.3 MPa at an A concentration of 0.5 %). This phenomenon suggests that the flexibility and ductility of FF can be modulated by adding A, resulting in variations in fiber thickness, diameter, and intermolecular interactions. Shavisi (2024) fabricated electrospun FF comprising chitosan-carrageenan with *Malva sylvestris* A and found that its tensile strength decreased from 11.02 MPa to 7.71 MPa while its elongation at break increased from 13.12 % to 30 % as A concentration increased from 0 % to 4 %.

3.2.5. Antioxidant properties

Fig. S2 presents the antioxidant activity of Z-FFs as a function of A addition (0.05–0.5 %). As anthocyanin (A) addition increased from 0.05 % to 0.5 %, antioxidant activity of Z-FF increased significantly from 84.49 % to 94.85 %, indicating their potential application for active food packaging. This phenomenon may be due to the increased A content (Table 2) in ZA-FF resulting from the naturally excellent antioxidant capacity of A for the inhibition of the DPPH radical (Khalafi et al., 2023). Kim et al. (2007) reported that the phenolic content of natural colorants was linearly correlated with antioxidant activity. Similar results were also found in Z-FF loaded with varying concentrations of anthocyanic extract of Jambolan (20–40 %; Dos Santos et al., 2023) and red onion

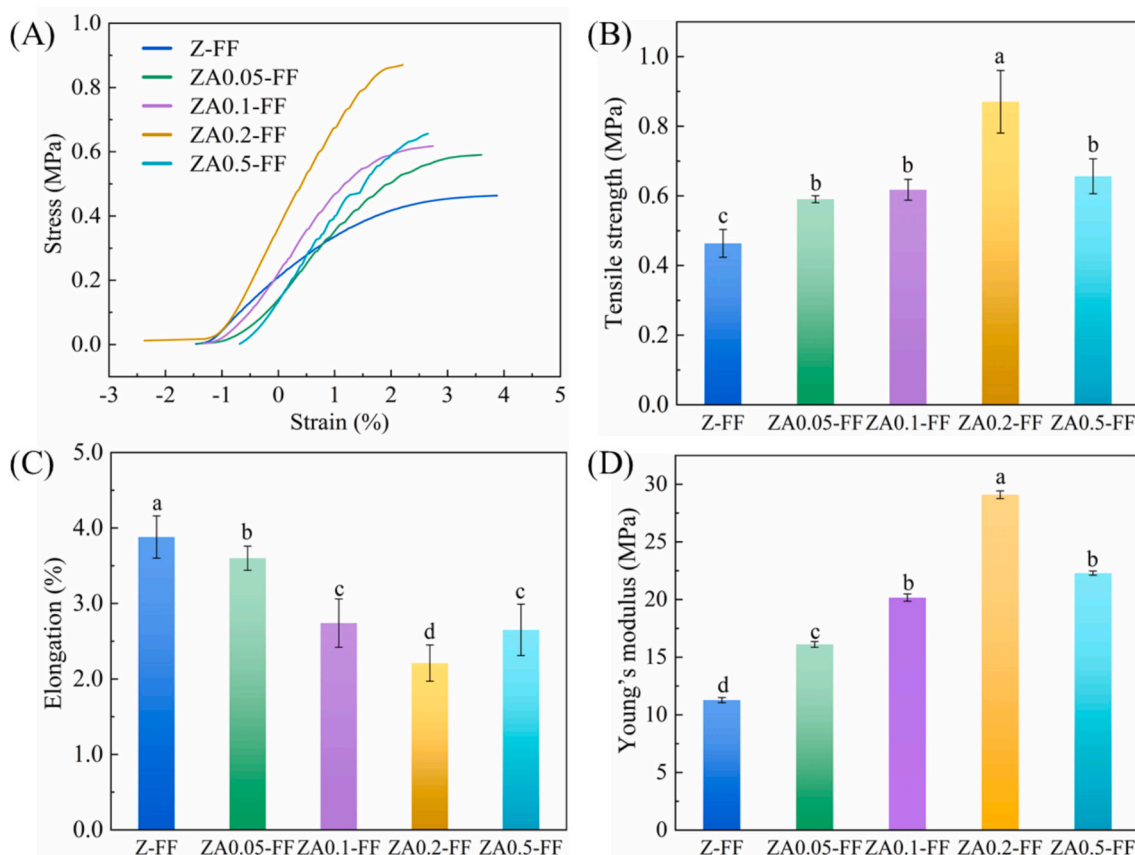


Fig. 3. Mechanical properties (A: stress-strain curves; B: tensile strength; C: elongation; D: Young's modulus) of Z-FFs as a function of A addition (0–0.5 %).

bulb extract (10–40 %; Cruz et al., 2024).

3.2.6. Storage stability

Fig. S3 exhibits the storage stability with heat and light of free A and Z-FFs as a function of A addition (0.05–0.5 %). Anthocyanin (A) retention values of all ZA-FFs were higher compared to free A during the storage with heat and light, indicating the enhanced A stability using the electrospinning approach. Under the environmental stress of heat and light, A retention of ZA-FF showed a gradual decrease as the concentration of A rose from 0.05 % to 0.5 %, which should be closely related to their A content in ZA-FF. Although A was more sensitive to light than heat (Enaru, Drețcanu, Pop, Stănilă, & Diaconeasa, 2021), A retention in ZA0.5-FF after 24 h of light could achieve ca. 90 %. Jiang et al. (2024) also found that electrospun pullulan/polyvinyl alcohol-FF incorporating bayberry pomace anthocyanin extract showed a good stability during storage at 25 °C for 20 days.

3.3. Color-responsiveness of FF to ammonia






The appearances and chromaticity characteristic values of Z-FF as influenced by A concentration (0–0.5 %) in an ammonia environment at 25 % (v/v) for 20 min are shown in Table 3. An apparent color change was noted in ZA-FF, with a significant decrease in L^* (91.6 to 81.0) and a significant increase in a^* , b^* , and ΔE (1.3 to 5.1; 9.8 to 11.4; 10.4 to 20.0) when the A concentration increased from 0.1 % to 0.5 %. This result was consistent with the yellow hue exhibited by A solution in an alkaline environment (Fig. S1) resulting from the formation of yellow chalcone (Chayavanich et al., 2023). Wu, Liu, Zhou, and Shao (2024b) also directly observed an obvious color change with changing ammonia concentrations in corn starch/polyvinyl alcohol films incorporation with blueberry A. A similar trend of color shift in response to ammonia vapor has been observed in starch-A-based pH-sensitive electrospun nanofiber mats (Lv et al., 2024). As reported previously, color changes are perceptible to the naked eye when ΔE exceeds 5 (Luchese, Abdalla, Spada, & Tessaro, 2018). The above result is comparable to that of corn starch/polyvinyl alcohol embedded with zirconium-based UiO-66 and anthocyanin-loaded ovalbumin-carboxymethylcellulose nanocomposites when exposed to 5 % ammonia vapor (Wu et al., 2024a). Therefore, the aforementioned results indicate Z-FF incorporated with A at concentrations of 0.2 % and 0.5 % hold promise as pH-sensitive freshness-indicating labels. Moreover, a reversible pH-sensing behavior to acid-ammonia cycle as reported from starch/chitosan-based film incorporated by anthocyanin-encapsulated amylopectin nanoparticles (Zheng, Liu, Yu, Farag, & Shao, 2023) should be followed in the future.

4. Conclusion

In this study, pH-sensitive, freshness-indicating labels based on ZA-FF were developed using green electrospinning technology. The addition of A modulated the thickness distribution, microscopic morphology, and fiber diameter distribution of electrospun Z-FF. The changes in secondary and crystal structures of ZA-FF likely contributed to their improved surface hydrophobicity, thermodynamic properties, and mechanical properties, with ZA0.2-FF and ZA0.5-FF exhibiting equivalent optimal functional performance. ZA-FF also showed a good antioxidant activity to DPPH radical and storage stability to environmental stress including heat and light. In addition, color changes in an ammonia environment were discernible to the naked eye owing to the high ΔE observed for Z-FF incorporated with A at concentrations of 0.2 % and 0.5 %. Despite this, the application in real food packaging for freshness indicating is necessary, which should be further clarified in the future work. This study provides novel insights into the design of Z-based freshness-indicating labels via electrospinning and is anticipated to stimulate further advancements in intelligent packaging for food products.

Table 3

Appearances and chromaticity characteristic values of Z-FFs as a function of A addition (0–0.5 %) subjected with ammonia environment.

Samples	Appearance	L^*	a^*	b^*	ΔE
Z-FF		96.6 ± 0.3 ^a	0.0 ± 0.1 ^e	8.8 ± 0.2 ^d	7.6 ± 0.1 ^e
ZA0.05-FF		94.0 ± 0.2 ^b	0.7 ± 0.0 ^d	9.4 ± 0.4 ^c	8.9 ± 0.5 ^d
ZA0.1-FF		91.6 ± 0.3 ^c	1.3 ± 0.1 ^c	9.8 ± 0.4 ^c	10.4 ± 0.5 ^c
ZA0.2-FF		88.3 ± 0.2 ^d	2.7 ± 0.1 ^b	10.3 ± 0.1 ^b	13.1 ± 0.2 ^b
ZA0.5-FF		81.0 ± 0.3 ^e	5.1 ± 0.1 ^a	11.4 ± 0.2 ^a	20.0 ± 0.3 ^a

CRedit authorship contribution statement

Jun Wang: Writing – original draft, Visualization, Methodology, Investigation, Funding acquisition, Data curation. **Wenpeng Zhao:** Writing – original draft, Methodology, Investigation. **Dongli Qin:** Methodology, Investigation. **Hongyan Shan:** Investigation, Formal analysis. **Xiaoman Zhu:** Investigation, Formal analysis. **Lilan Chen:** Writing – review & editing. **Ying Liu:** Writing – review & editing, Supervision, Project administration, Conceptualization. **Songnan Li:** Writing – review & editing, Supervision, Project administration, Methodology, Funding acquisition, Conceptualization.

Declaration of competing interest

The authors declare that they have no known competing financial interests or personal relationships that could have appeared to influence the work reported in this paper.

Acknowledgements

We gratefully acknowledge the support of a Project Funded by the Open Project Program of State Key Laboratory of Food Nutrition and Safety, Tianjin University of Science & Technology (No. SKLFNS-KF-202313), Natural Science Foundation of Jiangsu Province (BK20220585), “Shuangchuang” Doctor Talent Support Program of Jiangsu Province (JSSCBS20221323), China Postdoctoral Science Foundation (2022M712692), Yangzhou Key R&D Plan (Social Development) Project (YZ2022076), Yangzhou “Lvyangjinfeng” Talent Support Program (YZLYJFH2021YXBS172), and “QingLan” Talent Support Program of Yangzhou University.

Appendix A. Supplementary data

Supplementary data to this article can be found online at <https://doi.org/10.1016/j.fochx.2025.102163>.

Data availability

Data will be made available on request.

References

- Angel, N., Li, S., Yan, F., & Kong, L. (2022). Recent advances in electrospinning of nanofibers from bio-based carbohydrate polymers and their applications. *Trends in Food Science & Technology*, 120, 308–324.
- Aytac, Z., Ipek, S., Durgun, E., & Uyar, T. (2018). Antioxidant electrospun zein nanofibrous web encapsulating quercetin/cyclodextrin inclusion complex. *Journal of Materials Science*, 53, 1527–1539.

- Chayavanich, K., Kaneshige, R., Thiraphibundet, P., Furuie, T., Tamura, H., & Imyim, A. (2023). pH-responsive nanofibrous membrane fabricated from gelatin and red radish anthocyanins for meat spoilage monitoring. *Dyes and Pigments*, 216, Article 111331.
- Chen, H.-Z., Zhang, M., Bhandari, B., & Yang, C.-H. (2020). Novel pH-sensitive films containing curcumin and anthocyanins to monitor fish freshness. *Food Hydrocolloids*, 100, Article 105438.
- Ciarfaglia, N., Laezza, A., Lods, L., Lonjon, A., Dandurand, J., Pepe, A., & Bochicchio, B. (2021). Thermal and dynamic mechanical behavior of poly (lactic acid)(PLA)-based electrospun scaffolds for tissue engineering. *Journal of Applied Polymer Science*, 138 (44), 51313.
- Cruz, E. P. D., Pires, J. B., Jansen, E. T., Santos, F. N. D., Fonseca, L. M., Hackbart, H. C. D. S., & Dias, A. R. G. (2024). Electrospun nanofibers based on zein and red onion bulb extract (*Allium cepa*, L.): Volatile compounds, hydrophilicity, and antioxidant activity. *Journal of Food Science*, 89(3), 1373–1386.
- Dos Santos, F. N., De Souza, E. J. D., De Souza, J. F., Pires, J. B., Siebeneichler, T. J., Kringel, D. H., ... da Rosa Zavareze, E. (2023). Encapsulation of anthocyanin extract of jambolan (*Syzygium cumini* (L.)) in zein sub-micron fibers produced by electrospinning. *Food Biophysics*, 18(1), 133–147.
- Enaru, B., Dreţcanu, G., Pop, T. D., Stănilă, A., & Diaconeasa, Z. (2021). Anthocyanins: Factors affecting their stability and degradation. *Antioxidants*, 10(12), 1967.
- Erna, K. H., Rovina, K., & Mantihal, S. (2021). Current detection techniques for monitoring the freshness of meat-based products: A review. *Journal of Packaging Technology and Research*, 5(3), 127–141.
- Gao, R., Hu, H., Shi, T., Bao, Y., Sun, Q., Wang, L., Ren, Y., Jin, W., & Yuan, L. (2022). Incorporation of gelatin and Fe²⁺ increases the pH-sensitivity of zein-anthocyanin complex films used for milk spoilage detection. *Current Research in Food Science*, 5, 677–686.
- Garavand, F., Khodaei, D., Mahmud, N., Islam, J., Khan, I., Jafarzadeh, S., Tahergorabi, R., & Cacciotti, I. (2024). Recent progress in using zein nanoparticles-loaded nanocomposites for food packaging applications. *Critical Reviews in Food Science and Nutrition*, 64(12), 3639–3659.
- Gholizadeh, S., Almasi, H., Amjadi, S., Moradi, M., Ghadiri Alamdari, N., Salmasi, S., & Divsalar, E. (2024). Development and characterization of active packaging system based on zein nanofibers mat incorporated with geraniol-loaded nanoliposomes. *Food Science & Nutrition*, 00, 1–15. <https://doi.org/10.1002/fsn3.4180>
- Guo, Y., Wang, X., Shen, Y., Dong, K., Shen, L., & Alzalab, A. A. A. (2022). Research progress, models and simulation of electrospinning technology: A review. *Journal of Materials Science*, 1–47.
- Han, T., Xia, C., Huang, Y., Sun, C., Liu, D., Xu, W., & Wang, D. (2023). An electrospun sensing label based on poly (vinyl alcohol)-Ag-grape seed anthocyanidin nanofibers for smart, real-time meat freshness monitoring. *Sensors and Actuators B: Chemical*, 376, 132975.
- He, H., Song, Y., Li, M., Zhang, H., Li, J., Huang, H., & Li, Y. (2023). A novel anthocyanin electrospun film by caffeic acid co-pigmentation for real-time fish freshness monitoring. *Analytical Methods*, 15(2), 228–239.
- He, M., Jiang, H., Wang, R., Xie, Y., & Zhao, C. (2017). Fabrication of metronidazole loaded poly (ε-caprolactone)/zein core/shell nanofiber membranes via coaxial electrospinning for guided tissue regeneration. *Journal of Colloid and Interface Science*, 490, 270–278.
- Huang, X., Teng, Z., Xie, F., Wang, G., Li, Y., Liu, X., & Li, S. (2024). Loading of cinnamon essential oil into electrospun octenylsuccinylated starch-pullulan nanofiber mats: Electrospinnability evaluation, structural characterization, and antibacterial potential. *Food Hydrocolloids*, 148, Article 109426.
- Jiang, L., Wang, C., Zhao, F., Li, S., Sun, D., Ma, Q., & Jiang, W. (2024). Development of electrospun nanofiber films based on pullulan/polyvinyl alcohol incorporating bayberry pomace anthocyanin extract for aquatic products freshness monitoring. *Food Bioscience*, 58, Article 103717.
- Julien, T. C., Subramanyam, M. D., Katakam, H. C., Lee, S., Thomas, S., & Harmon, J. P. (2019). Ultrasoft polycarbonate polyurethane nanofibers made by electrospinning: Fabrication and characterization. *Polymer Engineering & Science*, 59(4), 838–845.
- Kailasa, S., Reddy, M. S. B., Maurya, M. R., Rani, B. G., Rao, K. V., & Sadasivuni, K. K. (2021). Electrospun nanofibers: Materials, synthesis parameters, and their role in sensing applications. *Macromolecular Materials and Engineering*, 306(11), 2100410.
- Khalafi, N., Gharachorloo, M., Ganjloo, A., & Yousefi, S. (2023). Electrospun zein nanofibers containing anthocyanins extracted from red cabbage (*Brassica oleracea* L.). *Journal of Food Science*, 88(11), 4620–4629.
- Khoshnoudi-Nia, S., Sharif, N., & Jafari, S. M. (2020). Loading of phenolic compounds into electrospun nanofibers and electrospayed nanoparticles. *Trends in Food Science & Technology*, 95, 59–74.
- Kim, M. J., Hyun, J. N., Kim, J. A., Park, J. C., Kim, M. Y., Kim, J. G., & Chung, I. M. (2007). Relationship between phenolic compounds, anthocyanins content and antioxidant activity in colored barley germplasm. *Journal of Agricultural and Food Chemistry*, 55(12), 4802–4809.
- Krumreich, F. D., Prietsch, L. P., Antunes, M. D., Jansen-Alves, C., Mendonça, C. R. B., Borges, C. D., ... d. R., & Zambiasi, R. C. (2019). Avocado oil incorporated in ultrafine zein fibers by electrospinning. *Food Biophysics*, 14, 383–392.
- Lee, H., & Yoon, Y. (2021). Etiological agents implicated in foodborne illness world wide. *Food Science of Animal Resources*, 41(1), 1.
- Li, S., Huang, L., Zhang, B., Chen, C., Fu, X., & Huang, Q. (2021). Fabrication and characterization of starch/zein nanocomposites with pH-responsive emulsion behavior. *Food Hydrocolloids*, 112, Article 106341.
- Li, S., Wang, C., Fu, X., Li, C., He, X., Zhang, B., & Huang, Q. (2018). Encapsulation of lutein into swelled cornstarch granules: Structure, stability and in vitro digestion. *Food Chemistry*, 268, 362–368.
- Li, Y., Zhu, J., Cheng, H., Li, G., Cho, H., Jiang, M., Gao, Q., & Zhang, X. (2021). Developments of advanced electrospinning techniques: A critical review. *Advanced Materials Technologies*, 6(11), 2100410.
- Li, Z., Weng, W., Ren, Z., Zhang, Y., Li, S., & Shi, L. (2022). Electrospun octenylsuccinylated starch-pullulan nanofiber mats: Adsorption for the odor of oyster peptides and structural characterization. *Food Hydrocolloids*, 133, Article 107992.
- Lova, P. (2021). Intelligent packaging for real-time monitoring of food-quality: Current and future developments. *Applied Sciences*, 11.
- Luchese, C. L., Abdalla, V. F., Spada, J. C., & Tessoro, I. C. (2018). Evaluation of blueberry residue incorporated cassava starch film as pH indicator in different simulants and foodstuffs. *Food Hydrocolloids*, 82, 209–218.
- Luduvico, K. P., Radünz, M., dos Santos Hackbart, H. C., Bona, N. P., Pedra, N. S., Schetinger, M. R. C., ... Stefanello, F. M. (2024). Electrospinning and electrospinning of tannic acid-loaded zein: Characterization and antioxidant effects in astrocyte culture exposed to E. Coli lipopolysaccharide. *International Journal of Biological Macromolecules*, 267, Article 131433.
- Luo, S., Saadi, A., Fu, K., Taxipalati, M., & Deng, L. (2021). Fabrication and characterization of dextran/zein hybrid electrospun fibers with tailored properties for controlled release of curcumin. *Journal of the Science of Food and Agriculture*, 101 (15), 6355–6367.
- Lv, H., Wang, C., He, D., Zhao, H., Zhao, M., Xu, E., Jin, Z., Yuan, C., Guo, L., & Wu, Z. (2024). Intelligent food tag: A starch-anthocyanin-based pH-sensitive electrospun nanofiber mat for real-time food freshness monitoring. *International Journal of Biological Macromolecules*, 256, Article 128384.
- Merz, B., Capello, C., Leandro, G. C., Moritz, D. E., Monteiro, A. R., & Valencia, G. A. (2020). A novel colorimetric indicator film based on chitosan, polyvinyl alcohol and anthocyanins from jambolan (*Syzygium cumini*) fruit for monitoring shrimp freshness. *International Journal of Biological Macromolecules*, 153, 625–632.
- Moradkhannejhad, L., Abdouss, M., Nikfarjam, N., Mazinani, S., & Heydari, V. (2018). Electrospinning of zein/propolis nanofibers; antimicrobial properties and morphology investigation. *Journal of Materials Science: Materials in Medicine*, 29, 1–10.
- Narayanan, V., Mani, M. K., & Thambusamy, S. (2020). Electrospinning preparation and spectral characterizations of the inclusion complex of ferulic acid and γ-cyclodextrin with encapsulation into polyvinyl alcohol electrospun nanofibers. *Journal of Molecular Structure*, 1221, Article 128767.
- Pakolpakçıl, A., Osman, B., Göktalay, G., Özer, E. T., Şahan, Y., Becerir, B., & Karaca, E. (2021). Design and in vivo evaluation of alginate-based pH-sensing electrospun wound dressing containing anthocyanins. *Journal of Polymer Research*, 28, 1–13.
- Panjagari, N., Raman, R., Uma, K., Suwalka, R., & Thomas, E. (2021). Freshness indicators for real-time quality evaluation of packaged animal origin foods: A mini-review. *Indian Journal of Animal Health*, 60(2), 153–166.
- Plath, A., Facchi, S., Souza, P., Sabino, R., Corradini, E., Muniz, E., Popat, K., Kipper, M., & Martins, A. (2021). Zein supports scaffolding capacity toward mammalian cells and bactericidal and antiadhesive properties on poly (ε-caprolactone)/zein electrospun fibers. *Materials Today Chemistry*, 20, Article 100465.
- Prietto, L., Mirapallete, T. C., Pinto, V. Z., Hoffmann, J. F., Vanier, N. L., Lim, L.-T., ... da Rosa Zavareze, E. (2017). pH-sensitive films containing anthocyanins extracted from black bean seed coat and red cabbage. *Lwt*, 80, 492–500.
- Rostamabadi, H., Assadpour, E., Tabarestani, H. S., Falsafi, S. R., & Jafari, S. M. (2020). Electrospinning approach for nanoencapsulation of bioactive compounds; recent advances and innovations. *Trends in Food Science & Technology*, 100, 190–209.
- Seong, Y., Mohammad, R., Byung, J., Dong-Wook, H., Joon, L., Jong, K., & Jeong, Y. (2016). Optimum conditions for the fabrication of Zein/ag composite nanoparticles from ethanol/H₂O co-solvents using electrospinning. *Nanomaterials*, 6(12), 230.
- Shavisi, N. (2024). Electrospun fiber mats based on chitosan-carrageenan containing *Malva sylvestris* anthocyanins: Physic-mechanical, thermal, and barrier properties along with application as intelligent food packaging materials. *International Journal of Biological Macromolecules*, 266, Article 131077.
- Shen, D., Zhang, M., Mujumdar, A. S., & Ma, Y. (2023). Consumer-oriented smart dynamic detection of fresh food quality: Recent advances and future prospects. *Critical Reviews in Food Science and Nutrition*, 1–21.
- Wan, Z., Wang, L., Yang, X., Guo, J., & Yin, S. (2016). Enhanced water resistance properties of bacterial cellulose multilayer films by incorporating interlayers of electrospun zein fibers. *Food Hydrocolloids*, 61, 269–276.
- Wang, H., Hao, L., Niu, B., Jiang, S., Cheng, J., & Jiang, S. (2016). Kinetics and antioxidant capacity of proanthocyanidins encapsulated in zein electrospun fibers by cyclic voltammetry. *Journal of Agricultural and Food Chemistry*, 64(15), 3083–3090.
- Wu, W., Liu, L., Zhou, Y., & Shao, P. (2024a). Highly ammonia-responsive starch/PVA film with gas absorption system as the 'bridge' for visually spoilage monitoring of animal-derived food. *Food Chemistry*, 430, Article 137032.
- Wu, W., Liu, L., Zhou, Y., & Shao, P. (2024b). Highly ammonia-responsive starch/PVA film with gas absorption system as the 'bridge' for visually spoilage monitoring of animal-derived food. *Food Chemistry*, 430, Article 137032.
- Zheng, L., Liu, L., Yu, J., Farag, M. A., & Shao, P. (2023). Intelligent starch/chitosan-based film incorporated by anthocyanin-encapsulated amylopectin nanoparticles with high stability for food freshness monitoring. *Food Control*, 151, Article 109798.